Wake length of an artificial seagrass meadow: a study of shelter and its feasibility for restoration

Villanueva, Raul[1,*]; Thom, Moritz[2]; Visscher, Jan[1]; Paul, Maike[1]; Schlurmann, Torsten[1]

[1]*Ludwig-Franzius Institute, Leibniz Universtät Hannover, Hannover, Germany*

[2]*Foschungszentrum Küste (FZK), Leibniz Universtät Hannover & Technische Universität Braunschweig, Hannover, Germany*

*Corresponding author: villanueva@lufi.uni-hannover.de

This is an Accepted Manuscript of an article published by Taylor & Francis in the *Journal of Ecohydraulics* on July 02 2021, available online: https://www.tandfonline.com/doi/10.1080/24705357.2021.1938256

This is an Accepted Manuscript of an article published by Taylor & Francis in the Journal of Ecohydraulics on July 02, 2021, by Villanueva et al.

Wake length of an artificial seagrass meadow: a study of shelter and its feasibility for restoration

Seagrasses are essential marine ecosystems for which restoration has proven challenging due to increased hydrodynamic stress. This study aims to analyze the flow alteration induced by an artificial seagrass (ASG) meadow by characterizing its wake effect through a shelter distance and thus yield guidance for seagrass restoration projects. Here, we define shelter distance as the longitudinal extent behind a meadow, with respect to the flow direction, where seagrass is protected and can hence grow successfully. Flume experiments were conducted for submerged meadows with three different lengths at constant canopy height, shoot density and water depth, and three different cross-section-averaged longitudinal flow velocities measured with state-of-the-art Particle Image Velocimetry (PIV). For the tested meadow morphology and hydrodynamic conditions, meadow length played a less important role regarding shelter distance, while incident flow velocity and effective canopy height governed the wake effect. Incident velocities <30 cm s^{-1} prompted shelter distances >2m behind the meadow, whereas higher velocities led to a reduced shelter distance ranging from 20-40 cm. ASG additionally produced an upwelling effect on the vertical distribution of the velocity profile observed along the wake, regardless of meadow length and incident velocity. Our results suggest that restoration projects should aim for areas of low flow, where currents induced by tidal or wind waves are less pronounced in order to activate larger shelter distances.

Keywords: Shelter distance; wake structure; flow-vegetation interaction; seagrass; ecosystem restoration

Introduction

Submerged Aquatic Vegetation (SAV) is a part of coastal and estuarine ecosystems, which in turn are essential for both human and wildlife (Barbier et al. 2011). Their ability to alter their surroundings has granted them the title of ecosystem engineers (Koch 2001; Bouma et al. 2005) and rendered them as an attractive supplement towards green engineering solutions for coastal protection (IPCC 2019; James et al. 2019; Seddon et al. 2020). Among these ecosystems are seagrass meadows which provide important ecosystem services such as nutrient cycling (Unsworth et al. 2019) and coastal protection (Ondiviela et al. 2014). Despite this, they have sustained a worldwide loss of at least 29% of the total surveyed cover due to climate-related and direct anthropogenic stress (Duarte 2002; Waycott et al. 2009). Therefore, seagrasses have been a focus of ecosystem restoration efforts through many studies and coastal ecosystem restoration projects over the past few decades (Fonseca et al. 1987; van Katwijk et al. 2000; van der Heide et al. 2007; Paling et al. 2009).

Van Katwijk et al. (2009; 2016) provide a comprehensive review of restoration efforts and present a guideline based on results from experiments and pilot studies.

Several factors were identified that affect the success rate of seagrass reestablishment and survival, such as the biotic environment (Unsworth et al. 2015), effectiveness of the reproduction mechanisms (McMahon et al. 2014), light availability (Orth et al. 2006; van der Heide et al. 2011) and hydrodynamic conditions (Fonseca and Bell 1998); the two latter represented the most defining ones (van Katwijk et al. 2016). Loss of seagrass leads to enhanced hydrodynamic conditions which in turn hinders restoration efforts for re-establishment (van Katwijk et al. 2000; van der Heide et al. 2007). Seagrass survival studies analyzing seed dispersal and cloning (Orth et al. 1994; McMahon et al. 2014; Statton et al. 2017) commonly recognize the importance of shelter, i.e. areas protected by aquatic vegetation, coral reefs and other aquatic structures against high current and wave loading. This calls for restoration strategies that provide shelter to enhance natural protection for seagrass in its early stages.

One lesser-known restoration approach is the use of synthetic structures akin to actual seagrass, i.e. artificial seagrass (ASG), which can provide shelter to growing meadows. ASG can mimic the physical properties of real seagrass, thus emulating services such as providing habitat for fauna (Bell et al. 1985) and promote seagrass growth within a small area it encloses (Tuya et al. 2017) through reduction of hydrodynamic forcing. This characteristic of ASG has been exploited within physical experiments regarding seagrass research (e.g. Bouma et al. 2005). However, the use of ASG for restoration has not been sufficiently studied. Carus et al. (in review) provide an insight into the current stance regarding this approach and show that much research is still needed. In this study, we focus on the effectiveness of ASG at providing shelter to promote seagrass growth, the target species being *Zostera marina*. Pilot restoration projects generally choose wave-sheltered areas (e.g. by other ecosystems), as seagrasses prefer such conditions (Barbier et al. 2011). We, therefore, focus on the seagrass-flow interaction and test the effect of meadow length on incident current reduction.

Shelter definition

Understanding the wake structure behind the seagrass meadow is essential for defining the shelter distance. Flow modulation in the wake of a meadow is a result of above-ground biomass (Paul 2018) and suggests that the extent of shelter along the wake depends on meadow morphology and the hydrodynamic conditions. However, a clear definition of shelter is not available in the literature for any specific meadow configuration. In the context of restoration, efficient shelter in the wake of ASG could be validated through the survival of seeds and seedlings deployed in and around the ASG. Shelter definition is complicated nonetheless as it depends on the target species to protect. In general, flow velocity should be reduced to levels which the target species can resist. The shelter distance will in turn depend on the incident velocity and ASG meadow morphology. Early studies on established and robust *Z. marina* have shown a tolerance for currents ranging from 120 - 150 cm s^{-1} (Fonseca et al. 1983). However, on growing SAV, Madsen et al. (2001) reported a beneficial range of current velocities as low as 0.02-0.06 cm s^{-1}, suggesting the current velocity around growing seagrasses should be drastically reduced. Koch et al. (2010) analyzed flow effects on seed movement of three different seagrass

species and showed that velocities of about 10 up to 25 cm s^{-1}, depending on sand grain size, allow for settlement and deposition. Orth et al. (1994) reported a critical bottom shear stress velocity of 0.7 cm s^{-1} (corresponding to flow velocity of 8 cm s^{-1}) for *Z. marina* seeds. These values provide threshold velocities that should not be exceeded in order to ensure the survival of growing meadows.

Flow structure within canopies of model aquatic vegetation has been widely studied (e.g. Gambi et al. 1990; Fonseca et al. 1983; Nepf and Vivoni 2000; Poggi et al. 2004). It has been shown that flow adjustment occurs along the meadow in the streamwise direction and depends on meadow morphology and hydraulic conditions (Chen et al. 2013). Further, wake effects have been analyzed by a handful of publications concentrating on flow structure characterization (Folkard 2005; Lefebvre et al. 2010; Chen et al. 2012; Zong and Nepf 2012; Hu et al. 2018). Most of these studies test flow velocities under 30 cm s^{-1}, utilizing Acoustic Doppler Velocimetry to build velocity profiles out of point measurements along the wake, with the furthest measurement usually ranging from 10 – 20 times the canopy height (for reconfigured flexible meadows). A comparison of studies and their respective initial model parameters, including this study, can be found in the supplementary Table S1. Here, we characterize the flow structure behind submerged meadows of different lengths up to a distance 100 times the reconfigured canopy height. Thereafter, we estimate the shelter distance of ASG meadows of different lengths under high (> 30 cm s^{-1}) incident unidirectional currents based on flow velocity thresholds of 10, 20 and 30 cm s^{-1}. The shelter distance is then the horizontal distance behind the meadow up to which the velocity threshold is not exceeded. Meadow density and plant mechanical properties were not varied and are not further discussed here.

Experimental set-up

The experiments were carried out in the circular track-flume at Ludwig-Franzius Institute of the University of Hanover, which comprises a width and a height of 1 m with cement plastered walls and smoothed concrete floor (for a detailed flume description, see Goseberg et al. 2013). Flow is generated by 4 pumps with an installed capacity of 16 kW, able to generate constant currents of up to 0.8 m s^{-1} in either direction. The recirculating flow passes through an 18-m-long horizontal and straight stretch, where model ASG was set up and the measurements were performed (Figure 1a). Flow straighteners were used to reduce swirls along the measuring area. At the center of the stretch, acrylic glass observation windows span along 3 m on both sides of the flume and aluminum plates make up the bed (covering a recession of the bed otherwise used to test different bed materials).

A state-of-the-art stereoscopic Particle Image Velocimetry (PIV) system from LAVISION GMBH was used here to measure 3D instantaneous velocities behind model ASG. Two CCD Imager ProSX 5MP-resolution cameras were located outside the flume on both sides, each looking through an observation window at an angle of 30° into the flume (Figure 1b). Image distortion caused by refraction was corrected through water-filled prisms whose outer planes were parallel to the viewing plane of the cameras. The

viewing angle of the cameras also created a distortion which was corrected during image post-processing utilizing LAVISION data acquisition and processing software DAVIS. The field of view (FoV) was formed within the illuminated area of a double-pulsed Nd:YAG laser expanded into a laser sheet parallel to the *x*-*z* plane, located 55 cm from one of the walls. Polyamide-12 seeding material (density 1.06 g cm^{-3} and diameter 50 μm) was used to visualize and measure flow velocity using PIV. Along the *x*-axis, the FoV was located in the center of the straight stretch following the window location (Figure 1a).

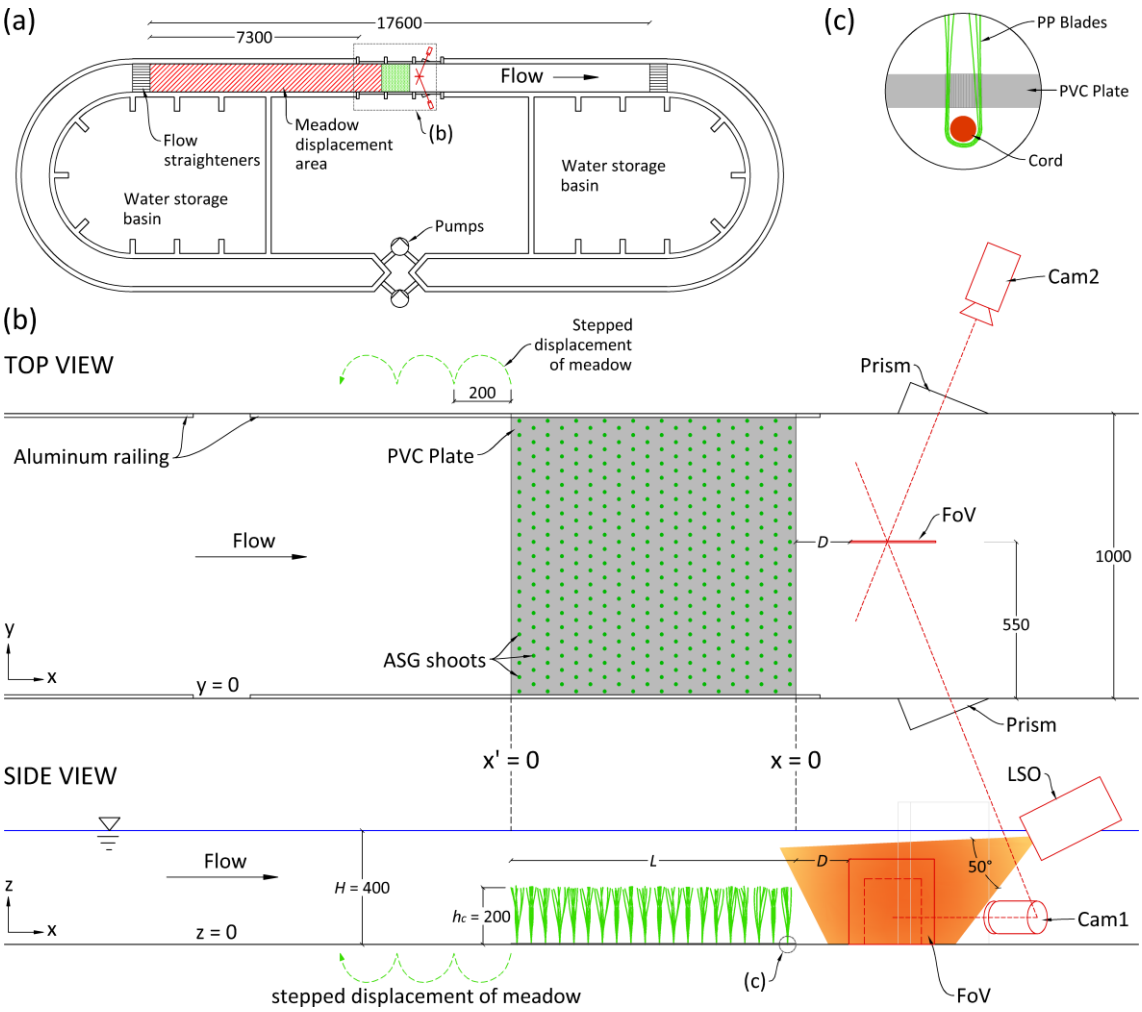

Figure 1. (a) Plan view of the recirculating flume. The diagonally hatched area indicates the section where the ASG meadows were displaced. (b) General set-up of stereoscopic PIV and cameras, with a 1-by-1-m ASG meadow. The dotted line within the field of view (FoV) shows the effective (cropped) 200x230-mm window extracted from each measurement. *x* and *x'* measure distance along the *x*-axis with 0 at the trailing and leading edge of the meadow, respectively. (c) Detail of shoot construction. Cords ran normal to flow and aligned to the rows of perforations in the PVC plate. All dimensions in mm. LSO: Light Sheet Optic.

Throughout the experiments, the *x*-axis corresponded to the streamwise direction with $x = 0$ at the trailing edge of the ASG meadow, regardless of the length; the *y*-axis to the spanwise direction (perpendicular to flow and parallel to the bed); and the *z*-axis vertical along the water column, with $z = 0$ at the bed (Figure 1b). An additional reference

point, *x'*, is given to mark the distance from the leading edge along the *x*-axis. The velocity components *u*, *v* and *w* correspond to the *x*, *y* and *z* directions, respectively. Throughout this study, the subscripts *0* and *k* indicate measurements at upstream and downstream positions, respectively. Each PIV measurement consisted of 500 dual-frame images taken at a frequency of 7 Hz (Δt = 0.143 s). A convergence analysis done for the instantaneous velocities as well as the resulting normal and shear stresses showed that 500 images sufficed for the purposes of this study, as these values were stable within that range. 3-Component – *u*, *v* and *w* – instantaneous velocity matrices (velocity fields) were produced for a 2D – *x*-*z* – plane with a size of 156x166 pixels. This corresponded to a size of 263x280 mm per dataset after image correction, which yielded a resolution of 1.6970 mm per pixel (in both *x* and *z*-directions).

The water depth was kept constant at H = 0.4 m. The incident streamwise velocity is described as input velocity u_o and corresponds to the bulk velocity measured in the flume at z = 25 cm, where no effect of the bed was observed. Control streamwise velocity measurements were done in the empty flume (no ASG) at different input velocities in order to calibrate the pumps and obtain control profiles to be contrasted with the velocities measured in the presence of ASG. The control average streamwise velocity profiles were used to calculate the shear velocity u_* (Table 1) and Coles' wake strength Π following the modified log-wake law (Equation 1, after Guo et al. 2005):

$$\frac{u_0 - u(z)}{u_*} = -\frac{1}{\kappa}\left(\ln \xi - 2\Pi \cos^2 \frac{\pi \xi}{2} + \frac{1-\xi^3}{3}\right) \quad (1)$$

where ξ is the relative distance from the wall and κ = 0.41 is the von Kárman constant.

In addition, measurements were also done directly in front of each meadow (FoV from *x'* = -20 cm to *x'* = 0) to obtain an upstream velocity field. Preliminary trials employing low streamwise velocities ranging from u_0 < 1 cm s^{-1} – 30 cm s^{-1} behind a 1-by-1-m patch were done to assess the effect of the ASG on flow and thus select 3 input velocities to be further analyzed for shelter. Analysis of the streamwise velocity along the wake showed that flow velocity reduction was more obvious for input velocities $u_0 \geq$ 20 cm s^{-1}. Nevertheless, a shelter effect could be seen for the whole range of input velocities, thus suggesting a significant service value for sheltering. As a result, higher input velocities of u_0 = 30, 45 and 60 cm s^{-1} were chosen to investigate the full wake development and test the limits of shelter capabilities of the chosen configurations; this provided a total of 9 different configurations to measure the wake flow. The channel Reynolds numbers, based on u_0 and channel geometry, ranged from 57,500-115,000.

Artificial Seagrass (ASG) meadows

Regarding restoration, an efficient ASG meadow is one with a density small enough to provide space for seagrass to grow and that does not reduce light availability, i.e. through blockage of light by the seagrass blades (shadowing). Therefore, a low shoot density λ = 390 shoots m^{-2} (compared to nature, e.g. Ondiviela et al. 2014; Fonseca et al. 2019) was chosen. ASG meadows were then produced using 4-mm-thick PVC plates as a base and

fixed to the bed by aluminum railings, which were also used to facilitate horizontal meadow displacement (Figure 1b). An alternating shoot placement pattern was chosen in order to avoid flow streams within the meadow, with a spacing S = 5 cm given by 5-mm perforations on the PVC plates. Each shoot consisted of 6 blades of polypropylene (PP; modulus of elasticity E = 1.49x10^8 Pa and density ρ = 0.9 g cm^{-3}) of width d = 5 mm, thickness b = 0.11 mm and length h_c = 200 mm assembled by folding 3 strips in half over a thin cord, then passing both ends through a perforation (Figures 1c and 2). In this study, h_c also represents the canopy height under no-flow condition, i.e. no blade reconfiguration. The dynamic similarity to real seagrass was tested using the buoyancy to rigidity ratio (λ_1 in Ghisalberti and Nepf 2002), which yielded a value of 0.44 s^2 m^{-1}. This value is higher than the 0.055 s^2 m^{-1} used by Ghisalberti and Nepf (2002), which best matched their target plant motion, due to the low E and ρ of PP; however, field values may range from 0.001 – 1 s^2 m^{-1} for different seagrasses (see Ghisalberti and Nepf 2002 and references therein for a detailed description of this parameter). The frontal area per canopy volume ($a = d\Delta S^{-2}$, as described in Nepf 2012a) was 2 m^{-1} at the base (blades superposed) and 12 m^{-1} at the top (all blades separated). For further calculations, a was taken as the average value over h_c, i.e. a = 7 m^{-1}, which resulted in a solid volume fraction ($\Phi = ab$, after Nepf 2012a) of Φ = 7.7x10^{-4}. A total of three 1x1-m ASG mats were fabricated in order to produce 3 meadow lengths L = 1, 2 and 3 m, after which flow reduction should be distinguishable (Fonseca et al. 1982), covering the full width of the flume.

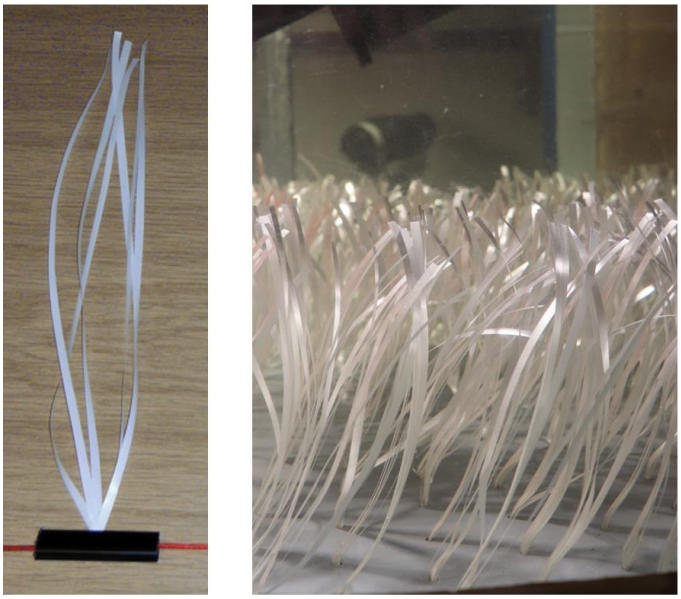

Figure 2. Model artificial seagrass (ASG) made of 3 strips of polypropylene (PP) bent in half and bound by a cord at the bottom. (left) 1 shoot; (right) submerged meadow.

The flexibility of PP ASG blades leads to reconfiguration, resulting in an effective canopy height h_r varying with velocity. h_r was determined manually by means of imagery taken during the experiments. A camera was fixed beside the flume directed orthogonally

toward one of the windows. For the 2-m-long meadow, 2 photographs and a 160-s-long video of the meadow under the influence of flow at all 3 tested velocities were taken prior to the PIV measurement. This was repeated for each run for as long as the meadow was visible through the observation window. A tape measure aligned vertically on the window was used to read the meadow height in each photograph under each velocity, thus obtaining h_r at 20-cm intervals from $x = 0$ to $x = 2$ m. The video was used to (qualitatively) observe plant sway and determine the plausibility of the taken tape measurement.

For the wake measurements, the ASG meadow was located upstream of the FoV. One FoV then corresponds to a flow field starting at a distance D downstream of the meadow (Figure 1b). The entire meadow was progressively displaced opposite the direction of flow at 20-cm intervals, i.e. D increased in 20-cm steps (overlap of around 5 cm between measurements), until it was no longer possible. Each step corresponded to one measurement and $x = 0$ moved synchronically with the ASG meadow so that the x position of the FoV increased 1 step size per measurement. This resulted in 357 datasets for all tested configurations. The streamwise centered location of the observation windows (and FoV) meant that meadow displacement was limited to the half distance of the flume. The length of the meadow itself also limited the maximum possible distance D to be measured, so that the PIV measurements were carried out until D = 840, 740 and 640 cm along the wake for the 1, 2 and 3-m long meadows, respectively.

Data analysis

Flow structure

The PIV output matrices were imported into MATLAB in order to extract velocity vectors and analyze flow development along the wake of the meadow. A smaller window of 200x230 mm was cropped out of each step-wise measurement. Each dataset consisted of three sets (one for each velocity component) of 500 matrices representing 500 instantaneous velocity fields (u, v and w) starting at each given distance D (Figure 1b) behind the meadow. Time-averaged statistics (mean, denoted by the overbar, i.e. $\bar{u}$, $\bar{v}$ and $\bar{w}$, and standard deviation) were calculated from the instantaneous velocity matrices. The fluctuating velocity components, denoted with a prime (u', v' and w'), were calculated by subtracting the mean from each instantaneous velocity. The computed fluctuating components were used to calculate Turbulent Kinetic Energy *TKE* using Equation 2. However, it is important to note that the employed sample size (500 images) and frequency (7 Hz), both subject to experimental limitations, are both too low for realistic, reliable estimation of turbulence. Higher frequency fluctuations, for example, cannot be detected. The depiction made here intends to provide a qualitative evaluation of the turbulence distribution and tendency along the wake of the meadow and should not be taken as a full characterization of the *TKE*.

$$TKE = \frac{1}{2}\left(\overline{u'}^2 + \overline{v'}^2 + \overline{w'}^2\right) \quad (2)$$

The flow structure within the flume is affected by the meadow starting at the leading edge (x' = 0 m). The streamwise velocity decelerates with increasing x' due to canopy drag, while the vertical velocity increases ($\overline{w}$ > 0 m s^{-1}) starting at the leading edge as the flow is redirected upwards and decays with increasing x' (Chen et al. 2013). $\overline{w}$ then reaches 0 at a distance described as the initial adjustment length X_D, which is a function of the canopy drag length scale L_c and the drag coefficient C_D. L_c has been adapted to aquatic canopies from analogies with surface vegetation interaction with atmospheric flows and is calculated as $L_c = 2(C_D a)^{-1}$ (for $\Phi < 0.1$, Nepf 2012a). Further, a mixing layer develops along the streamwise direction (Ghisalberti and Nepf 2002), therefore the flow structure at the trailing edge will vary for the different meadow lengths. Here, we characterize flow adjustment for the different test cases by comparing the mixing layer thickness, δ, at the trailing edge of each meadow. δ depends on the velocity at the top of the canopy U_{hr}, measured here at the trailing edge for each case; the flow velocity exiting the meadow U_1, measured here at the middle of the canopy layer, corresponding to the used a and Φ; and the velocity above the meadow, U_2, corresponding to the logarithmic profile (Equation 3, after Chen et al. 2013).

$$\delta = 2\left(\frac{\Delta U}{U_{hr}}\right) L_s \tag{3}$$

In (3), $\Delta U = U_2 - U_1$ and L_s is the shear length scale, which in turn depends on C_D. We calculated C_D from the stem Reynolds number Re_d and Φ using the empirical solution proposed by Tanino and Nepf (2008). Note that this empirical model was proposed after experiments with rigid cylinders as model vegetation. Here, we take flexibility into account by employing the reconfigured height h_r, as proposed by (Luhar and Nepf 2011). We calculated Re_d using the average measured near-bed flow velocity in front of the meadow up to half h_r, i.e. $\bar{u}(0 < z < 0.5h_r)$ at $x' = -0.5h_c$, and the single stem width d. We then calculate L_s and X_D with Equations 4 and 5, respectively (Chen et al. 2013). The center of δ was then set at a distance 0.5θ above h_r, where θ is the momentum thickness, as described by Ghisalberti and Nepf (2002).

$$\frac{L_s}{h_r} = 0.4(C_D a h_r)^{-1} \tag{4}$$

$$\frac{X_D}{L_C} = 1.5(1 + 2.3 C_D a h_r) \tag{5}$$

Finally, a simple quantification of the reduction of flow velocity, here described as attenuation ratio r_a, was done by integrating the area enclosed by the average streamwise velocity profiles ($A_{\bar{u}}$) up to $z = h_r$ utilizing Simpson's rule (Equation 6, newton-cotes quadrature rules) and the relative difference in flow velocity between upstream ($x' = -0.5h_c$) and downstream ($x = 0.5h_c$) using Equation 7. Note that r_a provides a comparison between flow upstream and downstream for $0 < z < h_r$ and does not reflect changes along the whole water column or along the spanwise dimension. r_a provides a simple quantification of the loss of velocity which, from continuity, can be seen in the

upper part of the profile. A summary of all calculated parameters including hydraulic conditions for our test cases is given in Table 1.

$$A_{\bar{u}} = \int_0^{h_c} \bar{u}\,(z)\,dz = \frac{1}{6}\sum_{n=1}^{N}(z_{n+1} - z_n)\left[\bar{u}(z_n) + 4\bar{u}\left(\frac{z_n+z_{n+1}}{2}\right) + \bar{u}(z_{n+1})\right] \quad (6)$$

$$r_a = \frac{A_{\bar{u},0} - A_{\bar{u},k}}{A_{\bar{u},0}} \quad (7)$$

Table 1. Experimental parameters for each test case calculated based on the respective reconfigured height h_r and solid volume fraction Φ = 0.00077 and a = 7 m^{-1}. The attenuation ratio r_a is given for $x = 0.5h_c$.

u_0 [cm s^{-1}]	L [m]	h_r [m]	u_* [m s^{-1}]	U_1 [m s^{-1}]	U_2 [m s^{-1}]	U_{hr} [m s^{-1}]	Re_d [-]	C_D [-]	L_s/h_r [-]	L_c [m]	X_D [m]	δ [m]	$r_a(h_r)$ [-]
	1	0.097	0.023	0.025	0.355	0.262	1.06E+02	1.367	0.432	0.209	0.980	0.105	0.587
30	2	0.097	0.021	0.016	0.363	0.161	7.05E+01	1.592	0.371	0.179	0.936	0.154	0.745
	3	0.097	0.024	0.027	0.378	0.167	1.15E+02	1.335	0.443	0.214	0.988	0.180	0.729
	1	0.083	0.032	0.053	0.521	0.410	2.28E+02	1.132	0.606	0.252	0.954	0.115	0.469
45	2	0.083	0.033	0.035	0.522	0.265	1.49E+02	1.241	0.553	0.230	0.920	0.169	0.731
	3	0.083	0.021	0.050	0.558	0.299	2.16E+02	1.144	0.600	0.250	0.950	0.170	0.650
	1	0.072	0.038	0.060	0.666	0.504	2.61E+02	1.106	0.721	0.258	0.882	0.124	0.480
60	2	0.072	0.046	0.054	0.680	0.372	2.34E+02	1.127	0.708	0.254	0.875	0.170	0.695
	3	0.072	0.023	0.069	0.713	0.364	2.97E+02	1.084	0.736	0.264	0.890	0.187	0.663

Shelter Distance

Vector stitching between datasets was applied to the calculated mean matrices to produce a full wake matrix for each configuration. The measured velocities were normalized by the corresponding input velocity. The positive effect of ASG on flow regarding shelter for restoration projects was interpreted and processed from the yielded data in two different ways: 1) the overall extent of the influence along the *x*-axis, which is defined here as the reach R_k, was obtained by calculating the difference between the upstream velocity field and the velocity fields at each step (Δu) whereby R_k represents the distance behind the meadow at which initial conditions, i.e. Δu = 0 m s^{-1} along the whole *z*-axis, were met; and 2) the span of continuous shelter provided by the meadow directly behind it along the *x*-axis, defined here as the shelter distance S_k, and determined for different threshold velocities chosen based on literature, as described below. Unfortunately, some PIV measurements showed inaccurate measurements near the bed due to high laser reflection. Considering this and that velocities near the bed are close to 0 due to bed friction, S_k, was set at the point along the *x*-axis where the mean velocity measured 3 cm above the bed exceeded the threshold velocity in order to be able to find a reliable and comparable value.

For R_k, Δu was calculated and graphically stitched together, thus providing an overview of the incremental velocity changes induced in the wake. However, the velocity

profile along the wake returns to normal conditions rather gradually, which complicates the identification of R_k and S_k. The latter is additionally subject to ambiguity in its definition as literature values correspond to different species of seagrass and boundary settings, with field conditions playing an important role when dealing with restoration (van Katwijk et al. 2016). For the analysis, three different velocity thresholds were chosen: 10, 20 and 30 cm s^{-1}. The first value complies with literature based on seed dispersal and settling studies (e.g. Koch et al. 2010). The second is a practical value for restoration projects, given that seeds and seedlings should be, within this context, initially buried in the bed (van Katwijk et al. 2016). The third threshold serves as a reference for areas with higher current velocities. The resulting values of $R_{k,90}$ (further described in the results) and S_k are given in Table 2.

Table 2 Summary of shelter distance results. Reach of the impact of the meadow up to 90% ($R_{k,90}$) normalized by h_c; Slopes of $R_{k,90}$ and the tailing influence of the meadow normalized by h_c; and Shelter distance (S_k) normalized by h_c for 3 incident velocities (denoted by the scalar subscript after S_k given in cm s^{-1}). Missing values under $S_{k,30}$ correspond to an unreadable S_k given that for u_0 = 30 cm s^{-1}, a threshold of likewise 30 cm s^{-1} cannot be surpassed.

u_0 [cm s^{-1}]	L [m]	$R_{k,90}/h_c$	$R_{k,90}$ Slope	Tailing Slope	$S_{k,10}/h_c$	$S_{k,20}/h_c$	$S_{k,30}/h_c$
30	1	17.69	0.021	0.011	3.65	12.2	-
	2	16.99	0.020	0.012	3.3	11.475	-
	3	17.16	0.018	0.013	2.625	10.425	-
45	1	15.99	0.025	0.008	0.9	2.5	9.35
	2	15.95	0.016	0.008	1.15	3.275	9.8
	3	17.16	0.025	0.010	0.95	3	8.85
60	1	12.33	0.028	0.012	0	1.075	3.175
	2	16.99	0.019	0.009	0.55	1.25	3.475
	3	15.12	0.028	0.006	0	1.275	3.25

Results

The control streamwise velocity profiles taken without the presence of ASG were compared with the upstream profiles ($x' = -0.5h_c$); this revealed no significant difference between these measurements. Figure 3 shows the profiles for u_0 = 30 cm s^{-1}, which were similar for all cases. Therefore, the effect of the meadow on flow was further characterized by the difference between downstream and upstream streamwise velocity, thus obtaining the calculated values of r_a and $R_{k,90}$ presented in Table 1 and Table 2, respectively.

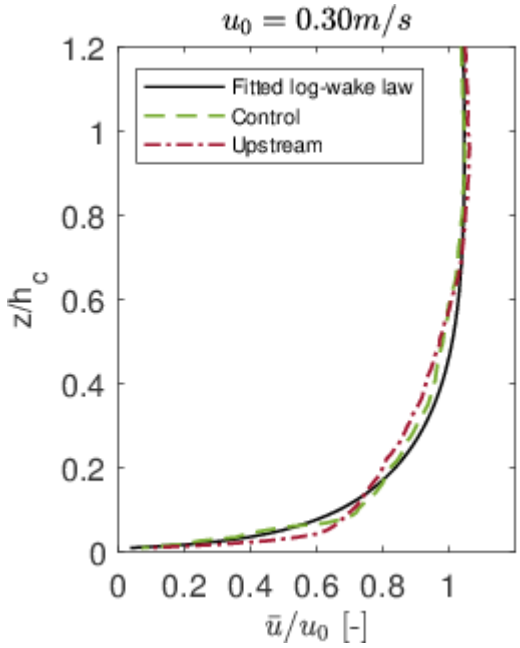

Figure 3. Comparison of the normalized control (no ASG) streamwise velocity profiles with those upstream (x' = -0.5h_c) of a 1-m meadow and the modified log-wake profile (Equation 1).

Measurements of effective canopy height h_r at 20 cm intervals revealed a gradual change in height depending on the position within the meadow (Figure 4), with the lowest heights (h_r = 5-6 cm) along the first 20cm. At 1 m (x' = 5h_c), a small peak was recorded for all cases, after which h_r remained relatively constant for the next meter. The small peak could be caused by the transition between mats (1x1-m each), but this cannot be proven with our measurements. For the purpose of simplicity, an average h_r was chosen to represent each input velocity u_0 based on the recorded heights from 1 to 2 m (Table 1).

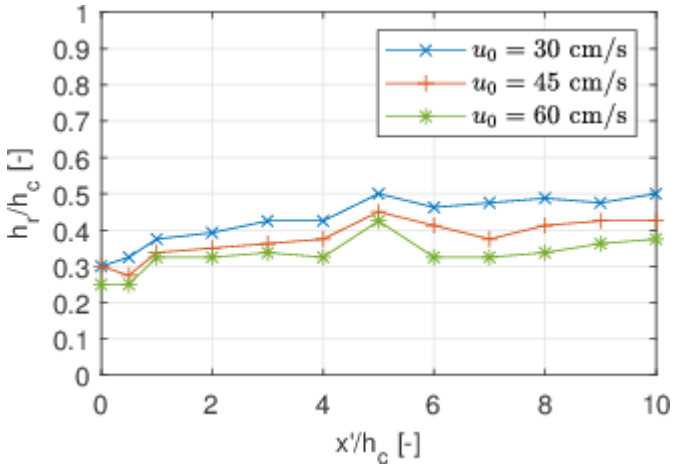

Figure 4. Evolution of effective canopy height h_r for the 2-m meadow for different input velocities u_0. x' is the distance from the leading edge of the canopy. Distances normalized by canopy height h_c.

Streamwise velocity and turbulent kinetic energy along the wake

The full wake vector field plots produced through matrix stitching showed a similar behavior among each other with regard to mean velocity $\bar{u}$ and *TKE* along the wake, regardless of meadow length and input velocity (Figure 5 shows the resulting wake measurement for one test case). Three major characteristics could be discerned for all cases: 1) a stark reduction of velocity in the area immediately behind the ASG meadow, especially up to $x/h_c = 5$ (i.e. 1 m) and quantified through r_a (Table 1); 2) an acceleration of flow above the canopy; 3) an approach to upstream conditions with increasing x.

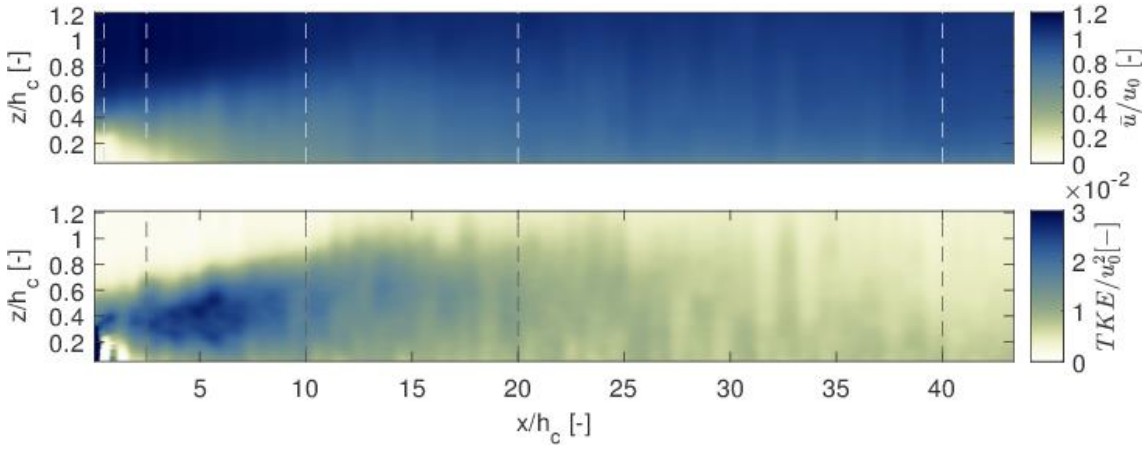

Figure 5. Mean streamwise velocity $\bar{u}$ (top) normalized by input velocity u_0 = 30 cm s^{-1} and turbulent kinetic energy *TKE* (bottom) normalized by u_0^2 along the full measured wake behind a 1-m ASG meadow. x and z are normalized by the canopy height h_c and measure from the trailing edge of the meadow and the bed, respectively. The dashed lines mark the positions where profiles in Figures 6 and 8 are shown.

The attenuation ratio r_a decreased with increasing velocity (Table 1). From r_a, attenuation is up to 70% at $x/h_c = 0.5$ for all input velocities. Interestingly, the meadow length L appears to play a role in the interface between 1 and 2 m, showing an increase between 15-25% in attenuation between L = 1 and 2 m, compared to a 1-8% difference between L = 2 and 3 m. Furthermore, for all tested configurations, the first 50 cm (x/h_c = 2.5) show significant flow reduction, hence shelter capability (Figure 6). A complete return to upstream conditions was not observable for any of the test cases, despite measuring up to $x = 90h_r$. Nevertheless, the velocity profiles at the far end of the measurable area within the wake (Figure 6) are very close to initial conditions yielding an r_a close to 1% for all configurations except two: L = 2 and 3 m for u_0 = 60 cm s^{-1}, which displayed a reduction of about 5%.

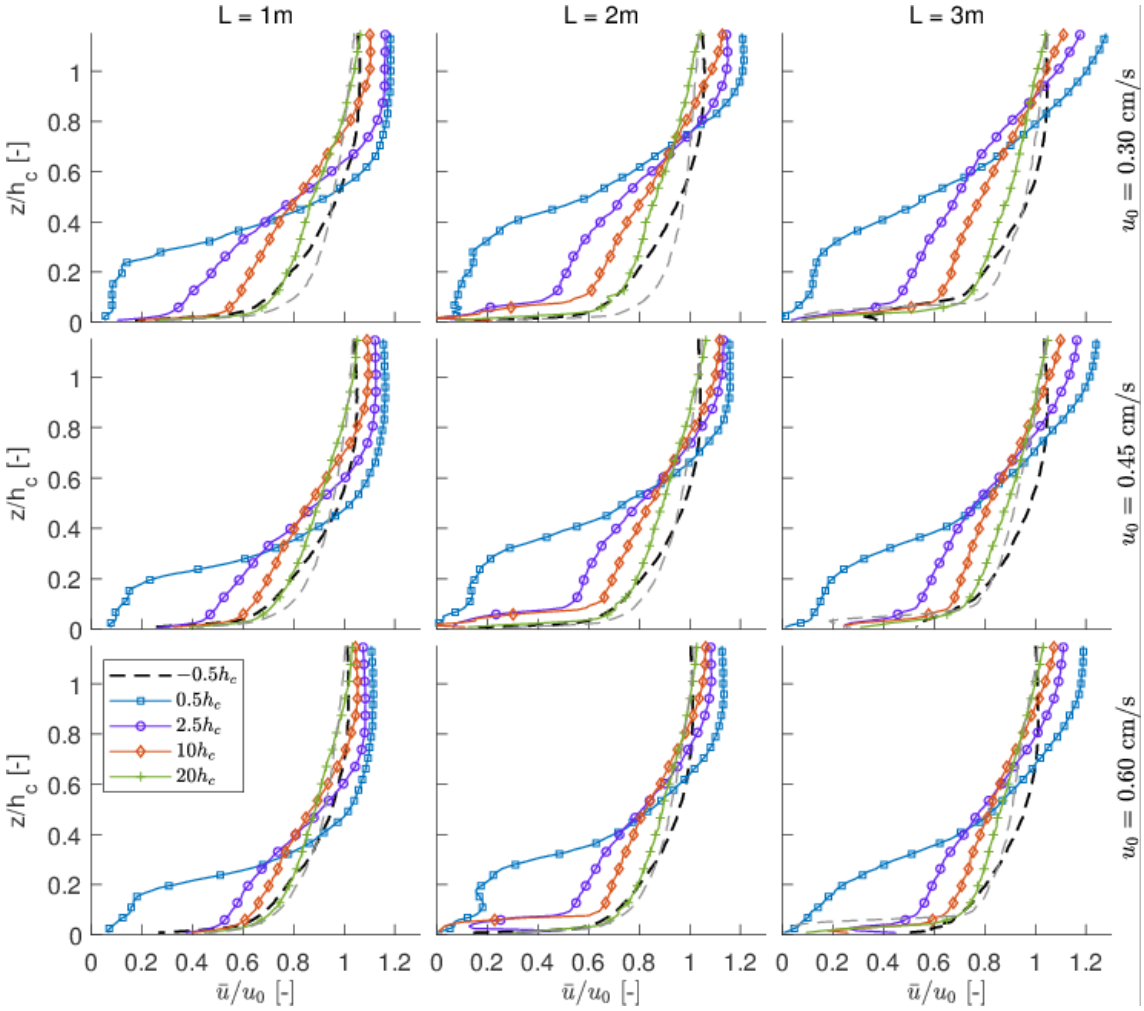

Figure 6. Profiles of mean streamwise velocity $\bar{u}$ at different positions in the wake of the meadow normalized by input velocity u_0. Subplot columns correspond to meadow lengths L and rows to input velocities. The gray dashed profiles correspond to positions at the far end of the measurement length D, i.e. x/h_c = 40, 35 and 30 for L = 1, 2 and 3 m, respectively.

The wake structure analyzed here shows the development after different flow conditions. Initial adjustment (X_D) for all cases was 75-90 cm (Table1). Note that X_D and the corresponding calculated values in Table 1 are not normalized. Considering the mixing layer as well, full adjustment of flow is then reached when the Reynolds stress ($-\overline{u'w'}$) at h_r is reached (Chen et al. 2013). Given that no measurements above the canopy were done, we compared the $-\overline{u'w'}$ ($z = h_r$) at the trailing edge of the canopy. For all cases, $-\overline{u'w'}$ increased with increasing meadow length, which means that a maximum $-\overline{u'w'}$ was not reached and flow in all cases is not fully developed. In natural canopies, this is also the case due to patchiness interrupting flow development (Rominger and Nepf 2011). Chen et al. (2013) proved that flow development and the canopy layer velocity at the trailing edge are not a function of meadow length. The mixing layer thickness δ, calculated utilizing Equation 3 at $x = 0.5h_c$, shows a similar behavior (Figure 7) as it

increases with increasing meadow length, whereby the change is smaller between L = 2 and 3 m as between 1 and 2 (this was also seen with the *TKE*). It is worth noting that despite δ begins to stabilize after x' = 2 m, the log region of the velocity profile continues to increase. Furthermore, the mixing layer penetrates to the bed for the highest input velocity when L > 1 m. In Figure 7, for u_0 = 30 cm s^{-1} and L = 3 m, the FoV did not show a return to the log profile.

Similarly to $\bar{u}$, the magnitude of *TKE* decreases further away from the meadow (Figure 8). In addition, the peak shifts upward (in z) with increasing L. We did a linear regression between the magnitude and z-position of the peak *TKE* (at x/h_c = 2.5) and meadow length and input velocity. High correlations were found between the *TKE* and u_0 and between the length and peak position (R^2 = 0.93 and 0.58, respectively), and poor correlations between *TKE* magnitude and L and between peak position and u_0. This suggests that the position of peak turbulence is affected by meadow length, rather than upstream velocity, but TKE can double in magnitude when doubling the velocity.

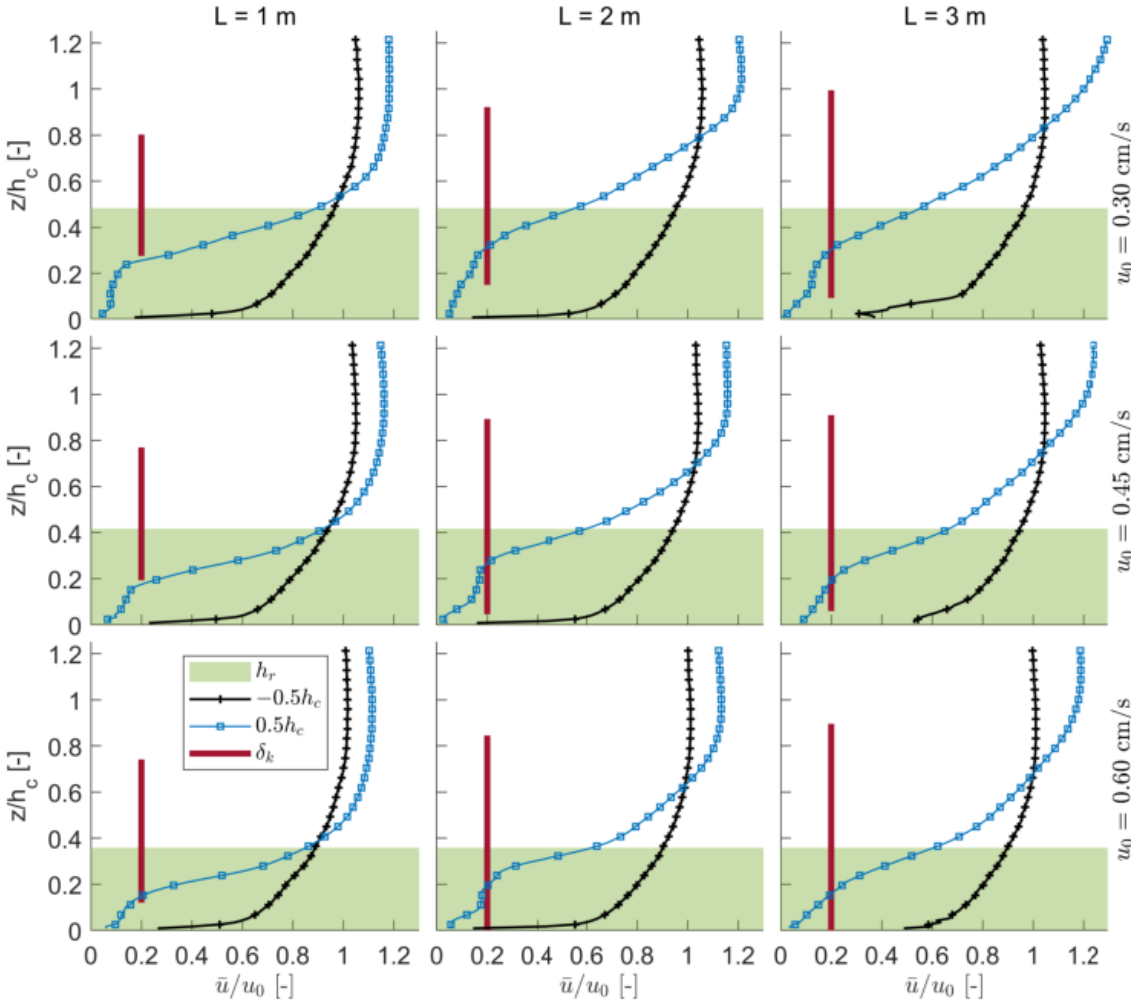

Figure 7. Mean streamwise velocity profile $\bar{u}$ normalized by input velocity u_0 at x' = -0.5h_c and x = 0.5h_c. The mixing layer thickness δ is shown as a vertical bar. Subscript k represents the wake. Subplot columns correspond to meadow lengths L and rows to input velocities u_0. The shaded area represents the effective canopy height h_r.

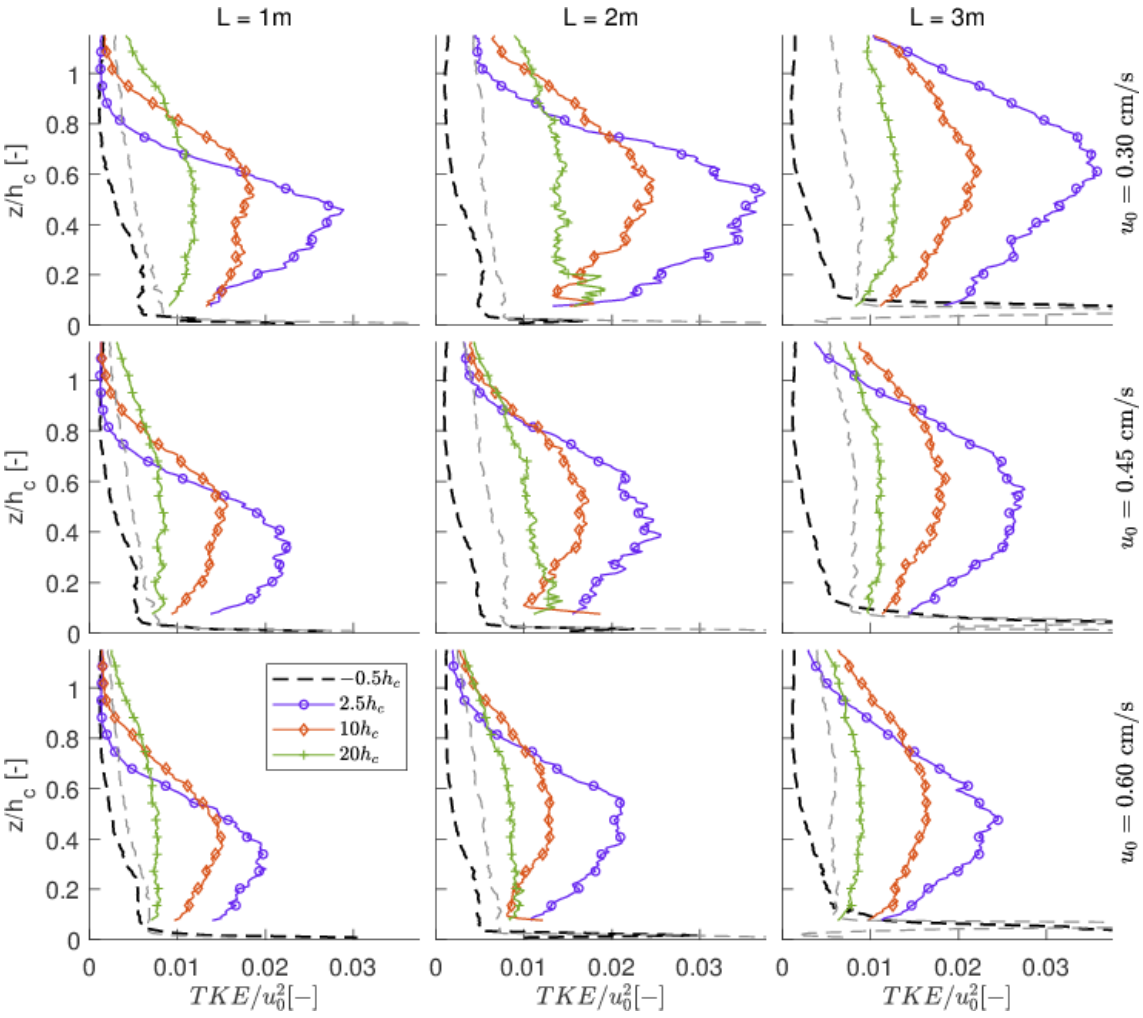

Figure 8. Profiles of turbulent kinetic energy *TKE* normalized by the squared input velocity (u_o^2) at different positions in the wake of the meadow. Columns correspond to meadow lengths *L* and rows to input velocities u_0. The gray dashed profiles show the positions at the far end of the measurement length *D*, i.e. x/h_c = 40, 35 and 30 for *L* = 1, 2 and 3 m, respectively.

Reach of meadow influence along the wake

The resulting flow field after calculating $\Delta\bar{u}$ along the whole wake shows that the length of the flume did not suffice to find a full return to upstream conditions. Figure 9 shows one configuration whereby all other run combinations displayed similar behavior. Nonetheless, an upwelling trend can be discerned following $\Delta\bar{u}$ along the wake showing 2 different slopes: one representing the increased influence of the meadow, directly behind it (darker red areas in Figure 9) and a slightly less pronounced slope following the minor influence that tails (tailing slope) the meadow along the full measured wake (light red tailing zone). The slopes were calculated by isolating the areas of reduced velocity (see Table 2) –i.e. the darker areas, shown for all configurations in Figure 10 –and

drawing a line through the center (for all cases, there is a distinctive transition zone between positive and negative values of Δu where $\Delta u \approx 0$). It is worth noting that with increasing distance along the wake a slight increase in velocity just above the bed is initiated (Figures 6 and 9). We hypothesize that this is caused by secondary currents coming from lateral parts of the section injecting additional momentum and that the low-velocity zone for $x/h_c > 10$ is not influenced by the coherent structures. This would also explain the lack of difference between L = 2 and 3 m, but the present data is not of sufficient resolution to verify this hypothesis.

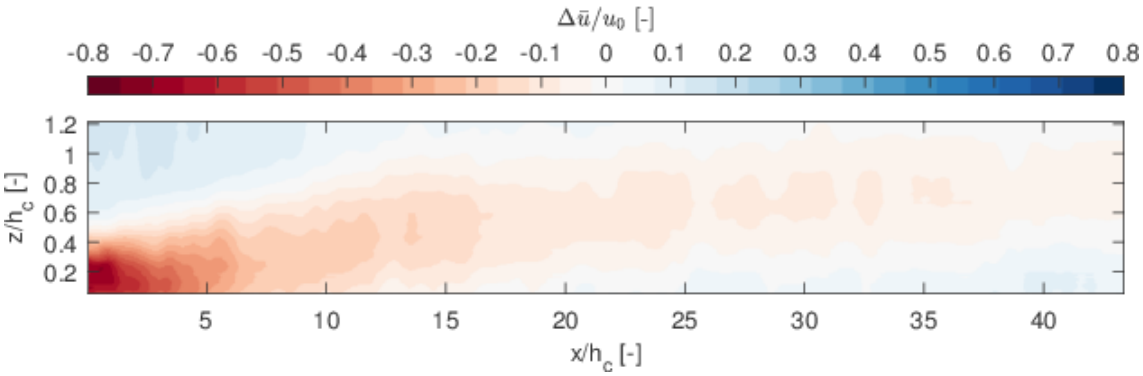

Figure 9. Differences in mean velocity ($\Delta\bar{u}$) along the wake of ASG normalized by incident velocity u_0 representing the reach (R_k) for L = 1 m and u_0 = 30 cm s^{-1}. x and z are normalized by the canopy height h_c and measure from the trailing edge of the meadow and the bed, respectively.

The tailing influence, i.e. the light red zone, observed in Figure 9 (which is similar in all cases, regardless of initial conditions) corresponds to the lowest values of $\Delta\bar{u}$. Therefore, to get a comparable quantity of R_k, a threshold of 90% was chosen, denominated $R_{k,90}$, so that all values portraying an absolute change in velocity less than 0.1 (10%) were set to 0 (Figure 10). The resulting $R_{k,90}$ values can be found in Table 2. Similar to the r_a within the canopy layer, the extent of the influence does not vary greatly with varying u_0 or between L = 2 and 3 m, compared to L = 1 and 2 m. At 1 m length, the meadow loses influence with increasing velocity. However, there is a minimum difference in reach between a 2 and 3-m meadow. Velocity plays a major role in $R_{k,90}$ for the 1-m meadow which follows the flow adjustment characteristics discussed earlier.

Along the z-axis, distribution of the non-zero $\Delta\bar{u}$ at the trailing edge of the meadow varies similarly to $R_{k,90}$ and h_r in that it increases with increasing L, decreases with increasing u_0, and shows a small variation between L = 2 and 3 m compared to that between L = 1 and 2 m. Like with the horizontal extent ($R_{k,90}$) velocity plays a more significant role at L = 1 m.

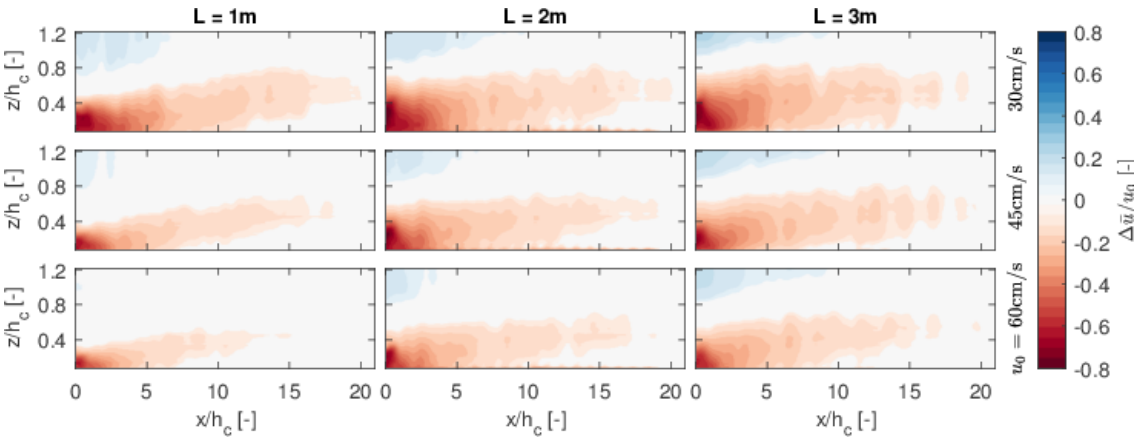

Figure 10. Contours of $\Delta\bar{u}$ up to 90% ($R_{k,90}$, i.e. reduction or increase above 10%) normalized by u_0. The x and z-axes begin at the trailing edge of the ASG meadow and the bed, respectively, and are normalized by the canopy height h_c. u_0 differs by row and L by column.

Sheltering distance

Mean velocities above the chosen velocity thresholds were removed from the full wake in order to identify S_k for each run under each respective threshold ($S_{k,10}$, $S_{k,20}$ and $S_{k,30}$, summarized in Table 2). Figure 11 shows $S_{k,20}$ for all run combinations, where it becomes obvious that the shelter area depends greatly on u_0. For an incident flow velocity of 30 cm s^{-1}, the ASG meadow is able to provide shelter, i.e. $\bar{u}$ < 20 cm s^{-1}, up to x/h_c = 12 (240 cm). At an input velocity higher than 30 cm s^{-1}, the meadow loses most of its shelter capacity, irrespective of the meadow length. S_k displays the same behavior for all thresholds (Table 2).

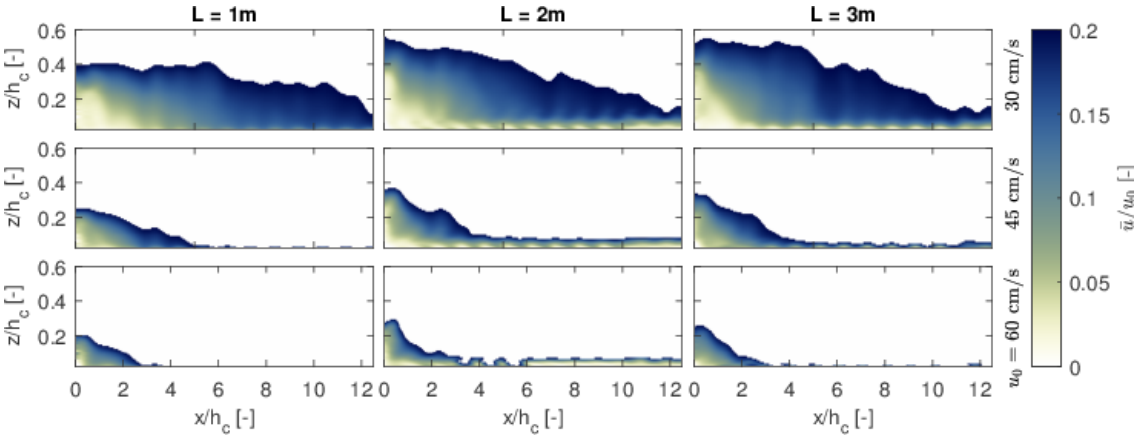

Figure 11. Flow fields along the wake for all configurations normalized by input velocity (u_0) showing the sheltered area for a threshold velocity of 20 cm s^{-1}. The white background represents an unsafe area for seagrass seeds and seedlings given the used velocity threshold. The x and z-axes begin at the trailing edge of the ASG meadow and the bed, respectively, and are normalized by the canopy height h_c. u_0 varies by row and L by column.

The lower velocity threshold of 10 cm s^{-1} shows very low shelter distances of less than 25 cm (x/h_c = 1.25) for the input velocities higher than 30 cm s^{-1} and only up to 75 cm (x/h_c = 1.25) for u_0 = 30 cm s^{-1}. On the other hand, a high-velocity threshold of 30 cm s^{-1} shows longer shelter distances for every input velocity (not measurable for u_0 = 30 cm s^{-1}), being on average $x = 9.3h_c$ and $3.3h_c$ (186.6 and 66 cm) for u_0 = 45 and 60 cm s^{-1}, respectively.

Discussion

The results suggest that the meadow has a marked effect on flow for all input velocities and meadow lengths. The meadow length L played a smaller role after reaching 2 m. Despite testing velocities higher in comparison to all cited studies, the effect on flow along the wake was uniform for all meadow lengths. This suggests that meadow density may play a more important role. Fonseca et al. (2019) recently suggested that meadow density in naturally occurring meadows is not a result of flow velocity and likewise, meadow density does not affect flow reduction within a meadow. This, however, contrasts with other studies where density plays a major role in flow adjustment (see e.g. Chen et al. 2012; Zong and Nepf 2012). Our study shows that even a highly porous and sparse meadow ($\Phi << 0.1$ and $a < 10$ m^{-1}) can effectively reduce flow velocity (up to 70%). Furthermore, the model for rigid vegetation from (Tanino and Nepf 2008), applied here for flexible vegetation utilizing the reconfigured height h_r, provided reliable results for the estimation of the drag coefficient (here $1.1 < C_D < 1.6$). We compared these results with assumptions from the literature, e.g. C_D = 1.95 tested by Luhar and Nepf (2011) and the more widely used assumption of C_D = 1 (Nepf 2012b), obtaining similar results regarding the initial adjustment length X_D (+10% for C_D = 1 and -10% for C_D = 1.95, on average), but lower boundary layer thickness δ (-25% on average) for the higher C_D. Increasing Φ had the same effect on X_D and δ, as C_D increases as well (Tanino and Nepf 2008), indicating that variations in meadow density, stem width and thickness play a more important role on flow adjustment compared to meadow length. Other studies suggest that reconfiguration, hence the flexibility of the material, plays an important role as well (Bouma et al. 2005; Luhar and Nepf 2011; Fonseca et al. 2019). Fonseca et al. (1982) and Paul and Gillis (2015) present models of canopy height against incident flow velocity for *Zostera marina* and *Zostera noltii* meadows utilizing average measured canopy heights. Given the important role of the canopy height, a relationship between h_r and the shelter distance S_k was developed (Figure 12). The aforementioned studies, among others, tend to record and report an effective canopy height with a constant value depending on current velocity, regardless of meadow length. However, as seen in Figure 4, meadow length can affect the average effective canopy height along the meadow, suggesting that further studies should take this into account when measuring h_r.

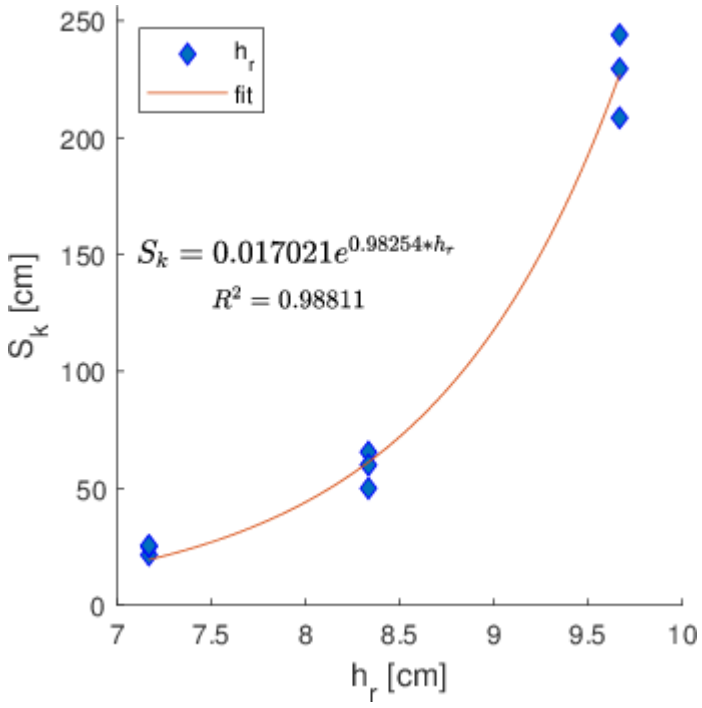

Figure 12. Relationship between effective canopy height h_r and shelter distance S_k along the wake. An exponential function of the form $y = ae^{bx}$ was fitted, yielding the given R^2. For the given coefficients, both parameters are to be given in cm.

As Figures 6 to 8 show, the velocity profile behind the meadow differs in its distribution along z for the different meadow lengths. It is interesting to note that, up to our measured height, the profile transitions from a pure mixing layer profile at $L \leq 2$ m (e.g. Ghisalberti and Nepf 2002) to a high-submergence-ratio hyperbolic tangent profile, as described by Nikora et al. (2013), at $L = 3$ m. The latter authors proposed a model that successfully predicts such vegetated flow profiles under fully developed flow by superposing canopy and boundary layer flow concepts, i.e. near-bed flow within the vegetation, the mixing layer and the boundary layer log and wake laws. Our profiles display a transition from the mixing layer profile to a profile including the boundary layer logarithmic profile when $L > 2$ m, which indicates that flow continues to develop even after a length of 2 m.

Flume experiments show *Z. marina* tolerance ranges between 5-100 cm s^{-1} with maximum bending angles at velocities above 40 cm s^{-1} (Fonseca et al. 1982). The results presented here confirm that after 40 cm s^{-1} there are lower differences observed (here between 45 and 60 cm s^{-1}) compared with the lowest tested velocity of 30 cm s^{-1}, regardless of meadow length. Additionally, studies have shown that a 1-m meadow is enough to observe a reduction of flow (Lefebvre et al. 2010; Fonseca et al. 1982), which can be confirmed here (Tables 1 and 2). Moreover, for restoration purposes, a 2-m meadow proves to be effective for sheltering and more feasible, given that the effect of the 3-m meadow is only slightly higher than that exhibited by the 2-m meadow.

Despite velocity being greatly reduced along the first few meters behind the meadow, turbulence is increased, which could pose a problem for seeds and seedlings.

As an example, Lefebvre et al. (2010) found that onset velocity for sediment motion behind a seagrass meadow was lower (< 20 cm s^{-1}) than for bare sand (20-23 cm s^{-1}), probably due to the increased turbulence, forming ripples up to a meter behind the meadow. This calls for further research on the velocity thresholds and their interaction with *TKE*. The high-resolution spatial measurement employed here allowed for the recognition of an upward trend in changes in velocity along the wake. This trend can also be observed in the distribution of the *TKE* (Figure 8), suggesting that *TKE* drives the wake structure behind a seagrass bed, whereby the meadow acts as an energy spreading filter on the whole water depth, despite the small *h/H* ratio used here. As such, it contributes to the dispersion and upwelling of the incident current profile by the production of wake vortices and a larger portion of turbulence to the flow field. The upwelling displayed two slopes –which could be separated at the 90%-reach of the influence of the meadow ($R_{k,90}$) –and an injection of momentum in the lower part for $x > 10h_c$ (Figure 6 and 8). The slope is greater between the trailing edge of the meadow and the $R_{k,90}$, but continues steadily positive along the rest of the measured stretch.

Finally, our calculated shelter distance yielded values ranging from 2 to 25 times the reconfigured canopy height h_r (or up to 10 times the canopy height h_c , Table 2), analogous to terrestrial studies, which have reported $2.5h_c$ for forest canopies (Detto et al. 2008). In aquatic canopies, Hu et al. (2018) demonstrated a strong correlation between eddy formation along the wake and sediment deposition. This, coupled with the shelter distance defined here for different threshold velocities, depending on target species to protect, could help improve the chances of success within restoration projects.

Conclusions

This study analyzed the effect of artificial seagrass (ASG) on flow, focusing on the wake structure and its development behind meadows of 3 different lengths under 3 different unidirectional current velocities. The meadows were of a constant shoot density of 390 shoots m^{-2} and submergence ratio of 0.5 (under no-flow conditions). The objective was to analyze the shelter capacity of ASG given a certain shelter threshold velocity which can theoretically allow seeds and seedlings used in the framework of restoration projects to grow successfully.

We found that a meadow of length $1 < L < 2$ m parallel to the mean flow direction is enough to reduce flow velocity up to 70% (within the height covered by the ASG). The reduction obtained by larger meadows falls within a similar magnitude and is thus not proportional to the possible costs of assembling patches longer than 2 m. Nevertheless, a longer meadow can decrease bending and thus shift the turbulence peaks upwards, which is beneficial for settling seeds. Even a highly flexible ASG meadow with low density can provide shelter for seedlings up to 10 times the canopy height h_c behind the meadow; nevertheless, a higher stiffness is recommended to reduce reconfiguration, which in turn could increase the shelter area. Furthermore, reconfiguration as a function of length needs to be better studied. Finally, regardless of length, density and incident velocity, an ASG meadow creates an upwelling reduction of flow which goes on par with the turbulence distribution. Further research is encouraged to describe the effects along the full water

column. It is important to note that these results are for the specific chosen material and comparison with other materials would provide a better idea of the importance of meadow mechanical properties within the context of morphology and shelter.

Acknowledgements

This study was part of the collaborative project “SeaArt - Long term establishment of SEAgrass ecosystems through biodegradable ARTificial meadows", funded by Niedersächsisches Vorab and MWK – Federal state of Lower Saxony (Grant No. ZN3187). We would like to thank the anonymous reviewers whose comments significantly improved this manuscript. Likewise, we thank Mareike Taphorn for her help during the preparation phase of the experiments and Luise Hentze for her set up of the PIV system and preliminary study.

Disclosure statement

No potential conflict of interest Q1 was reported by the authors.

Funding

This study was part of the collaborative project “SeaArt – Long term establishment of SEAgrass ecosystems through biodegradable ARTificial meadows," funded by Niedersєachsisches Vorab and MWK – Federal state of Lower Saxony (Grant No. ZN3187).

Supplementary material

Table S1. Studies dealing with wake structure in within the context of aquatic vegetation. *Used live vegetation; $^{+}$ tested also (or $^{++}$ only) patches not spanning the full flume width. a: upright height, i.e., for flexible canopies, the extended leaf; b: average reconfigured height.

Study	Instrument	Model Vegetation	Submergence state	Water Depth [m]	Patch Length [m]	Patch Width [m]	Canopy height [m]		Furthest distance measured along wake		
							a	b	[m]	ratio to a	ratio to b
Lefebvre et al. (2010)	ADV	Flexible*	Submerged	0.4	0.5 - 2.25	0.15 - 0.3^{+}	0.23 - 0.28	0.12 - 0.18	2.5	8.9 - 10.87	13.88 - 20.83
Folkard (2005)	ADV	Flexible	Submerged	0.35	1	0.9	0.5	0.175	2.4	4.8	13.71
Zong & Nepf (2012)	ADV	Rigid	Emergent	0.133	0.12 - 0.42	0.12 - 0.42	0.133	-	9	67.67	-
Chen et al. (2013)	ADV	Rigid	Submerged	0.14 - 0.28	1.5 - 4.8	1.2	0.07	-	0.5	7.14	-
Chen et al. (2012)	ADV	Rigid	Emergent	0.133	0.05 - 0.42	0.05 - 0.42^{++}	0.133	-	9	67.67	-
Hu et al. (2018)	ADV	Flexible	Submerged	0.14	0.1	0.1 - 0.4^{+}	0.13 - 0.28	0.065 - 0.07	0.8	2.86 - 6.15	11.42 - 12.31
This study	PIV	Flexible	Submerged	0.4	1 - 3	1	0.2	0.072 - 0.097	8.4	42	86.6 - 116.7

References

Barbier EB, Hacker SD, Kennedy C, Koch EW, Stier AC, Silliman BR. 2011. The value of estuarine and coastal ecosystem services. Ecol Monogr. 81(2):169–193.

Bell JD, Steffe AS, Westoby M. 1985. Artificial seagrass. How useful is it for field experiments on fish and macroinvertebrates? J Exp Mar Biol Ecol. 90 (2):171–177.

Bouma TJ, de Vries MB, Low E, Peralta G, Tánczos IC, van de Koppel J, Herman PM. 2005. Trade-offs related to ecosystem engineering: a case study on stiffness of emerging macrophytes. Ecology. 86(8):2187–2199.

Carus J, Arndt C, Schr€oder B, Thom M, Villanueva R, Paul M. 2021. Using artificial seagrass for promoting positive feedback mechanisms in seagrass restoration. Front Mar Sci. 8:546661

Chen Z, Jiang C, Nepf H. 2013. Flow adjustment at the leading edge of a submerged aquatic canopy. Water Resour Res. 49(9):5537–5551.

Chen Z, Ortiz A, Zong L, Nepf H. 2012. The wake structure behind a porous obstruction and its implications for deposition near a finite patch of emergent vegetation. Water Resour Res. 48(9):W09517

Detto M, Katul GG, Siqueira M, Juang J, Stoy P. 2008. The structure of turbulence near a tall forest edge: the backward-facing step flow analogy revisited. Ecol Appl. 18(6):1420–1435.

Duarte CM. 2002. The future of seagrass meadows. Envir Conserv. 29(2):192–206.

Folkard AM. 2005. Hydrodynamics of model Posidonia oceanica patches in shallow water. Limnol Oceanogr. 50(5):1592–1600.

Fonseca MS, Bell SS. 1998. Influence of physical setting on seagrass landscapes near Beaufort, North Carolina, USA. Mar Ecol Prog Ser. 171:109–121.

Fonseca MS, Fisher JS, Zieman JC, Thayer GW. 1982. Influence of the seagrass, *Zostera marina L.*, on current flow. Estuar Coast Shelf Sci. 15(4):351–364.

Fonseca MS, Thayer GW, Kenworthy WJ. 1987. The use of ecological data in the implementation and management of seagrass restorations. Fla Mar Res Pub. 42: 175–187

Fonseca MS, Fourqurean JW, Koehl MAR. 2019. Effect of seagrass on current speed: importance of flexibility vs. shoot density. Front Mar Sci. (6):376

Fonseca MS, Zieman JC, Thayer GW, Fisher JS. 1983. The role of current velocity in structuring eelgrass (*Zostera marina L.*) meadows. Estuar Coast Shelf Sci. 17(4):367–380.

Gambi MC, Nowell ARM, Jumars PA. 1990. Flume observations on flow dynamics in *Zostera marina* (eelgrass) beds. Mar Ecol Prog Ser. 61(1/2):159–169.

Ghisalberti M, Nepf HM. 2002. Mixing layers and coherent structures in vegetated aquatic flows. J Geophys Res C Oceans. 107(C2):3–1–3-11.

Goseberg N, Wurpts A, Schlurmann T. 2013. Laboratoryscale generation of tsunami and long waves. Coast Eng. 79:57–74.

Guo J, Julien PY, Meroney RN. 2005. Modified log-wake law for zero-pressure-gradient turbulent boundary layers. J Hydraul Res. 43(4):421–430.

Hu Z, Lei J, Liu C, Nepf H. 2018. Wake structure and sediment deposition behind models of submerged vegetation with and without flexible leaves. Adv Water Res. 118:28–38.

[IPCC] Intercontinental Panel on Climate Change. 2019. IPCC special report on the ocean and cryosphere in a changing climate. Geneva (Switzerland). IPCC.

James RK, Silva R, van Tussenbroek BI, Escudero-Castillo M, Mari~no-Tapia I, Dijkstra HA, van Westen RM, Pietrzak JD, Candy AS, Katsman CA, et al. 2019. Maintaining tropical beaches with seagrass and algae: a promising alternative to engineering solutions. BioScience. 69(2):136–142.

Koch EW. 2001. Beyond light: physical, geological, and geochemical parameters as possible submersed aquatic vegetation habitat requirements. Estuaries. 24(1):1–17.

Koch EW, Ailstock MS, Booth DM, Shafer DJ, Magoun AD. 2009. The role of currents and waves in the dispersal of submersed angiosperm seeds and seedlings. Restor Ecol. 18(4):584–595.

Lefebvre A, Thompson CEL, Amos CL. 2010. Influence of Zostera marina canopies on unidirectional flow, hydraulic roughness and sediment movement. Continent Shelf Res. 30(16):1783–1794.

Luhar M, Nepf HM. 2011. Flow-induced reconfiguration of buoyant and flexible aquatic vegetation. Limnol Oceanogr. 56(6):2003–2017.

Madsen JD, Chambers PA, James WF, Koch EW, Westlake DF. 2001. The interaction between water movement, sediment dynamics and submersed macrophytes. Hydrobiologia. 444 (1/3):71–84.

McMahon K, van Dijk K-j, Ruiz-Montoya L, Kendrick GA, Krauss SL, Waycott M, Verduin J, Lowe R, Statton J, Brown E, et al. 2014. The movement ecology of seagrasses. Proc R Soc B. 281(1795):20140878.

Nepf HM. 2012a. Flow and transport in regions with aquatic vegetation. Annu Rev Fluid Mech. 44(1):123–142.

Nepf HM. 2012b. Hydrodynamics of vegetated channels. J Hydraul Res. 50(3):262–279.

Nepf HM, Vivoni ER. 2000. Flow structure in depth-limited, vegetated flow. J Geophys Res. 105(C12):28547–28557.

Nikora N, Nikora V, O'Donoghue T. 2013. Velocity profiles in vegetated open-channel flows: combined effects of multiple mechanisms. J Hydraul Eng. 139(10):1021–1032.

Ondiviela B, Losada IJ, Lara JL, Maza M, Galv an C, Bouma TJ, van Belzen J. 2014. The role of seagrasses in coastal protection in a changing climate. Coast Eng. 87: 158–168.

Orth RJ, Luckenbach ML, Marion SR, Moore KA, Wilcox DJ. 2006. Seagrass recovery in the Delmarva Coastal Bays, USA. Aquat Bot. 84(1):26–36.

Orth RJ, Luckenbach ML, Moore KA. 1994. Seed dispersal in a marine macrophyte: implications for colonization and restoration. Ecology. 75(7):1927–1939.

Paling EI, Fonseca MS, van Katwijk MM, van Keulen M. 2009. Coastal wetland restoration and management: seagrass restoration. In: Perillo GME, editor. Coastal wetlands: an integrated systems approach. 1st ed. Amsterdam: Elsevier. p. 687–713.

Paul M. 2018. The protection of sandy shores – can we afford to ignore the contribution of seagrass? Mar Pollut Bull. 134:152–159.

Paul M, Gillis LG. 2015. Let it flow: how does an underlying current affect wave propagation over a natural seagrass meadow? Mar Ecol Prog Ser. 523:57–70.

Poggi D, Porporato A, Ridolfi L, Albertson JD, Katul GG. 2004. The effect of vegetation density on canopy sub-layer turbulence. Boundary Layer Meteorol. 111(3):565–587.

Rominger JT, Nepf HM. 2011. Flow adjustment and interior flow associated with a rectangular porous obstruction. J Fluid Mech. 680:636–659.

Seddon N, Daniels E, Davis R, Chausson A, Harris R, Hou-Jones X, Huq S, Kapos V, Mace GM, Rizvi AR, et al. 2020. Global recognition of the importance of nature-based solutions to the impacts of climate change. Glob Sustain. 3:e15

Statton J, Montoya LR, Orth RJ, Dixon KW, Kendrick GA. 2017. Identifying critical recruitment bottlenecks limiting seedling establishment in a degraded seagrass ecosystem. Sci Rep. 7(1):1–12.

Tanino Y, Nepf HM. 2008. Laboratory investigation of mean drag in a random array of rigid, emergent cylinders. J Hydraul Eng. 134(1):34–41.

Tuya F, Vila F, Bergasa O, Zarranz M, Espino F, Robaina RR. 2017. Artificial seagrass leaves shield transplanted seagrass seedlings and increase their survivorship. Aquat Bot. 136:31–34.

Unsworth RKF, Collier CJ, Waycott M, McKenzie LJ, Cullen-Unsworth LC. 2015. A Framework for the resilience of seagrass ecosystems. Mar Pollut Bull. 100(1): 34–46.

Unsworth RKF, McKenzie LJ, Collier CJ, Cullen-Unsworth LC, Duarte CM, Eklof JS, Jarvis JC, Jones BL, Nordlund LM. 2019. Global challenges for seagrass conservation. Ambio. 48(8):801–815.

van der Heide T, van Nes EH, Geerling GW, Smolders AJP, Bouma TJ, van Katwijk MM. 2007. Positive feedbacks in seagrass ecosystems: implications for success in conservation and restoration. Ecosystems. 10(8):1311–1322.

van der Heide T, van Nes EH, van Katwijk MM, Olff H, Smolders AJP. 2011. Positive feedbacks in seagrass ecosystems – evidence from large-scale empirical data. PLos One. 6(1):e16504.

van Katwijk MM, Bos AR, de Jonge VN, Hanssen LSAM, Hermus DCR, de Jong DJ. 2009. Guidelines for seagrass restoration: importance of habitat selection and donor population, spreading of risks, and ecosystem engineering effects. Mar Pollut Bull. 58(2):179–188.

van Katwijk MM, Hermus DCR, de Jong DJ, Asmus RM, de Jonge VN. 2000. Habitat suitability of the Wadden Sea for restoration of *Zostera marina* beds. Helgol Mar Res. 54(2-3):117–128.

van Katwijk MM, Thorhaug A, Marbà N, Orth RJ, Duarte CM, Kendrick GA, Althuizen IHJ, Balestri E, Bernard G, Cambridge ML, et al. 2016. Global analysis of seagrass restoration: the importance of large-scale planting. J Appl Ecol. 53(2):567–578.

Waycott M, Duarte CM, Carruthers TJB, Orth RJ, Dennison WC, Olyarnik S, Calladine A, Fourqurean JW, Heck KL, Hughes AR, et al. 2009. Accelerating loss of seagrasses across the globe threatens coastal ecosystems. Proc Natl Acad Sci USA. 106(30):12377–12381.

Zong L, Nepf H. 2012. Vortex development behind a finite porous obstruction in a channel. J Fluid Mech. 691:368–391.